Low-temperature magnetic susceptibility of Si:P in the nonmetallic region

K. Andres,* R. N. Bhatt, P. Goalwin,† T. M. Rice, and R. E. Walstedt
Bell Laboratories, Murray Hill, New Jersey 07974
(Received 30 December 1980)

Measurements of the phosphorus donor susceptibility $\chi_D(T)$ in Si:P have been made using a superconducting quantum interference device at phosphorus concentrations from 1×10^{17} to 4×10^{18} cm^{-3} over the temperature range from 2 mK to 4 K and in applied magnetic fields down to 10 Oe. Above $T\sim30$ mK a plot of $\ln\chi_D$ vs $\ln T$ shows a roughly linear characteristic with a slope which diminishes with increasing concentration. For $T<30$ mK χ_D is found to level off in an unexpected fashion in that the temperature at which this occurs is relatively independent of concentration. The leveling is less pronounced at 10 Oe for the most dilute sample; however, this sample exhibits an anomalously large saturation effect in 50 Oe. The leveling of χ_D cannot reasonably be attributed to hyperfine effects or to magnetic ordering as a consequence of interdonor exchange interactions. Susceptibility calculations are presented which are based on *a priori* exchange couplings between many-valley orbital ground states for the donors. In the spherical approximation for the envelope functions, the exchange integral is the product of a rapidly varying interference factor and an isotropic factor which can be obtained from variational calculations for the hydrogen molecule. Calculations of $\chi_D(T)$ have been carried out using both a pair approximation modified to take account of larger clusters and a computer-simulation cluster analysis which includes an error estimate based on a molecular-field approximation. The molecular-field approximation is described in detail here for the first time. The two methods of calculation are in mutual agreement and in good accord with the data down to $T\sim30$ mK, where modified pair corrections are small. The calculations yield values of envelope function radius and donor concentration in good agreement with other experimental and theoretical estimates.

I. INTRODUCTION

In the past two decades, a sizable body of experimental data has been collected on the electronic properties of doped semiconductors. These materials undergo a transition from metallic to nonmetallic (insulating) behavior at impurity concentrations below some critical value.[1] Thus for Si:P the electrical resistivity is observed to diverge at low temperatures[2] for donor (P) concentration $n_D \lesssim 4\times10^{18}/\text{cm}^3$, indicating that electrons at the Fermi level have become localized. It is only at still lower concentrations ($n_D < 1\times10^{18}/\text{cm}^3$) that the donor electrons in the insulating ground state can be considered to be in essentially hydrogenic $1s$ orbitals around individual phosphorus ions.[3] In this case the magnetic properties of the system can be described in terms of a system of localized spins ($s=\frac{1}{2}$) coupled by hydrogenic exchange interactions which are random in magnitude, but uniformly antiferromagnetic in character. Moreover, using molecular-hydrogen calculations[4,5] as a guide, the exchange interactions can be quantitatively characterized.

The low-temperature magnetic properties of such an "amorphous antiferromagnet" are of interest for several reasons, a general one being the currently wide interest in the behavior of amorphous systems. The exchange-coupled donors have several features in common with spin-glasses as well as some interesting differences. It is one of the main points of this work to search for spin-glass ordering in a doped semiconductor. Our conclusion in brief is negative, but certain anomalous behavior is found at very low temperatures which, however, is quite different from that of conventional spin-glasses.

In considering common features doped semiconductors have with spin-glasses, the primary one is that such systems are magnetically disordered with competing exchange bonds. Thus, there is no way to arrange the spins to satisfy all bonds or to produce long-range magnetic order. Many systems of this nature are found to exhibit the susceptibility peak characteristic of spin-glasses.[6] The present systems differ from conventional spin-glasses in that the spins are $s=\frac{1}{2}$, the interactions are purely antiferromagnetic, and the strength of the nearest-neighbor exchange interaction ranges over several orders of magnitude. It is not clear which of these differences is responsible for the apparent lack of spin-glass ordering. We consider this question further in Sec. V.

The present magnetic susceptibility studies were carried out using a superconducting-quantum-

interference-device (SQUID) magnetometer in a dilution refrigerator, with demagnetization cooling employed for temperatures below 20 mK. Experimental details are given in Sec. II. Measurements were made at temperatures ranging from 4K down to 3 mK in fields as low as 10 G. Donor concentrations ranged from 1×10^{17} up to $4 \times 10^{18}/\text{cm}^3$. Extremely careful work was required to subtract correctly the large diamagnetic background susceptibility of the silicon host.

Previous work[7,8] on Si:P was limited to higher concentrations and temperatures $T > 1$ K. The only study comparable to the present one is that of In-doped CdS,[9] in which magnetization measurements were carried out using Faraday rotation techniques over a temperature range 70 mK $\leq T \leq 2$ K. The latter measurements reached the percolation threshold[10] of the donor spins, but were limited to relatively high field ($H_0 \sim 1$ kG). The present measurements on Si:P, presented in Sec. III, extend to well below the percolation threshold of all but the lowest concentration sample and are in much lower fields.

The strength of the exchange interactions was obtained from calculation of molecular hydrogen as was done previously for CdS, with an additional modification to include the rapidly varying interference factors appropriate to indirect-gap semiconductors. The magnetic properties of the random exchange Hamiltonian are calculated in two different ways, as described in Sec. IV. A modified pair approximation[11] is presented in detail here for the first time. This modification enables us to include the effect of larger clusters in an approximate way and substantially improves the low-temperature behavior. In addition, a numerical cluster analysis of simulated random distributions similar to that used in previous work[9] is also reported. This method is believed to give accurate results where the molecular field corrections are small, and is used to test the accuracy of the modified pair approximation. These methods of calculation agree with each other and, using *a priori* values of the exchange interactions, give excellent agreement with experiment over a wide temperature range. Both methods are essentially limited to higher temperatures and deviate from experiment at $T < 30$ mK. Neither method is capable of predicting a transition to a state with "frozen-in" spin orientations such as the spin-glass state. The comparison between experiment and theory is discussed in Sec. V.

II. EXPERIMENTAL

A. General considerations

P-doped Si samples (uncompensated) grown from the melt were obtained from various sources[12] (see Table I). The phosphorous concentration of all samples was determined from their room-temperature resistivities using the Irvin curve.[2,3] Since the susceptibility measurements must be done in low fields, the SQUID technique is ideally suited for this purpose. Two cryostats were used, one to cover the temperature range from 1.1 to 4.2 K, and another (a dilution refrigerator with a nuclear magnetic cooling stage) for the lower temperatures.

B. Cryostat for the 1.1 to 4.2 K region

The measuring system, which is located in a pumped helium bath, consists of a superconducting field coil and a pair of astatically wound pickup coils inside it, into which the samples can be dipped for absolute magnetization measurements. The arrangement is shown schematically in Fig. 1. All coils are wound onto concentric Be-Cu forms which fit tightly into each other and are securely fastened to the lower part of a quartz tube (0.9 cm i.d.), which contains the

TABLE I. List of parameters for all samples investigated. Values of n_D are obtained from the Irvin curve (see Ref. 2). a^* and n_{theor} are values of the Bohr radius and concentration, respectively, used in the calculations. Δ is the cluster threshold employed in the computer simulation studies. The initials W.E. and G.D. refer to Western Electric Co. and the General Diode Co., respectively. Values of a^* can be varied by ±3% and n_{theor} by ±10%, in a correlated fashion, without seriously affecting fits.

Sample	Origin	ρ(295 K) (Ω cm)	n_D ($10^{17}/\text{cm}^3$)	a^* (Å)	n_{theor} ($10^{17}/\text{cm}^3$)	Δ (mK)
A	Recticon Co.	0.086	1.1	17.2	1.07	12.5
B	W.E.	0.037	4.3	15.2	4.25	25.0
C	G.D.	0.029	7.2	15.2	7.1	25.0
D	G.D.	0.022	12	15.4	11	
E	G.D.	0.012	37			

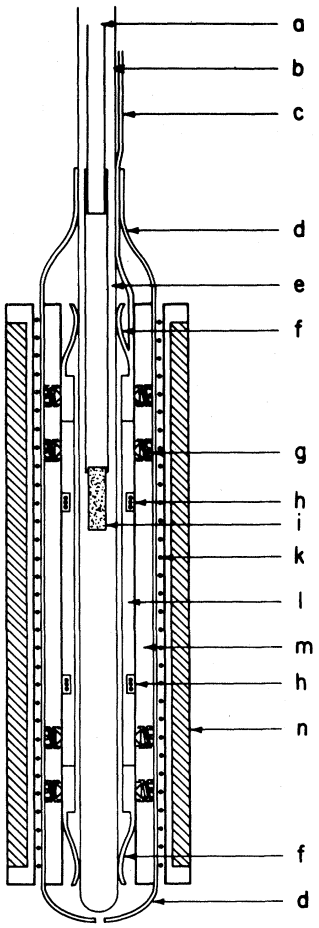

FIG. 1. Magnetometer for the 1.1 to 4.2 K temperature region. (a) Fiber rod, (b) quartz tube, (c) lead capillary with SQUID lead, (d) lead shield, (e) mylar cylinder, (f) Be-Cu springs, (g) Be-Cu locking screws, (h) SQUID pickup coils, (i) sample, (k) lead shield heater, (l) coil form, (m) Be-Cu spacer, and (n) field coil.

sample holder. The Nb pickup coils (10 turns each) are directly connected to a SQUID sensor via a lead capillary tube. Measurements are done by first freezing a field of 300 Oe into the lead shield (using the built-in lead shield heater) and then dipping the sample in and out of the upper pickup coil while monitoring the flux change. The samples were always in the shape of prisms of approximate dimensions $0.38 \times 0.38 \times 1.3$ cm^3. An absolute calibration of the SQUID system is obtained by dipping into the pickup coils a rectangular cross section one-layer copper coil of the same dimensions. Passing a current through this coil generates the same magnetic field as that of a uniform magnetic dipole density inside it. The magnetic form factor is thus properly taken into account with this calibration. Working with this cryostat in the range between 1.1 and 4.2 K, great care was taken to avoid spurious signals from the sample holder or from oxygen impurities. Only pure helium gas out of liquid storage containers was used as a thermal exchange gas. After trying out many sample holder materials, the best results were obtained by wrapping a 0.38-cm diameter cylinder out of clear thin mylar foil, attaching one end of it to a fiber holder and sticking the samples to the other end of it with a dab of fresh Duco cement. In this way, the bare sample could be lowered into the coil, and it was not necessary to subtract any empty holder signal. When measuring such weak signals in low magnetic fields, one is very susceptible to ferromagnetic dust particles on the surface of the sample. Reproducible results could only be obtained on freshly etched samples. "Older" samples always showed evidence of a small amount of surface ferromagnetism (as could be determined from the field dependence), the origin of which is still unclear.

C. Adiabatic demagnetization cryostat

To obtain data below 1 K, a moving-coil magnetometer was built into a dilution refrigerator, as shown schematically in Fig. 2(a). The arrangement is based on the same measuring principle as described above, except that now the two samples attached to the copper coldfinger remain stationary and the coil system is moved. In the neutral position shown in Fig. 2(a), the two pickup coils "see" only the high-purity copper coldfinger, whose signal thus cancels. In an upper position, the upper sample dips into the upper coil and in a lower position, one can observe the magnetization of the lower sample. The system is calibrated the same way as described above. With the dilution refrigerator alone, end temperatures of 15 mK can be reached. Lower temperatures are generated by nuclear adiabatic demagnetization of 30 g of $PrNi_5$, which is soldered to the lower end of the coldfinger (see Ref. 13 for a review of this technique). It should be pointed out that absolute measurements are only possible in the absence of the nuclear cooling stage, since the superconducting magnet constitutes too much of a disturbance for the magnetometer, in spite of the fact that there is a superconducting shield around the pickup coils. Care was taken to build the magnetometer suspension out of nonmagnetic material (mostly lead-free brass) and to avoid superconducting solder joints in its vicinity, in order to minimize spurious signals when moving the coils. To avoid warmup effects during this process, it was found important to take off any mechanical load from the guidance wheels of the coil assembly (the wheel bearings are made out of graphite and have 0.127-cm-diameter stainless-steel axles). The coil assembly is therefore symmetrically suspended with silk threads and counterbalanced at the top, as shown in Fig. 2(b). Also indicated in this figure is the opto-

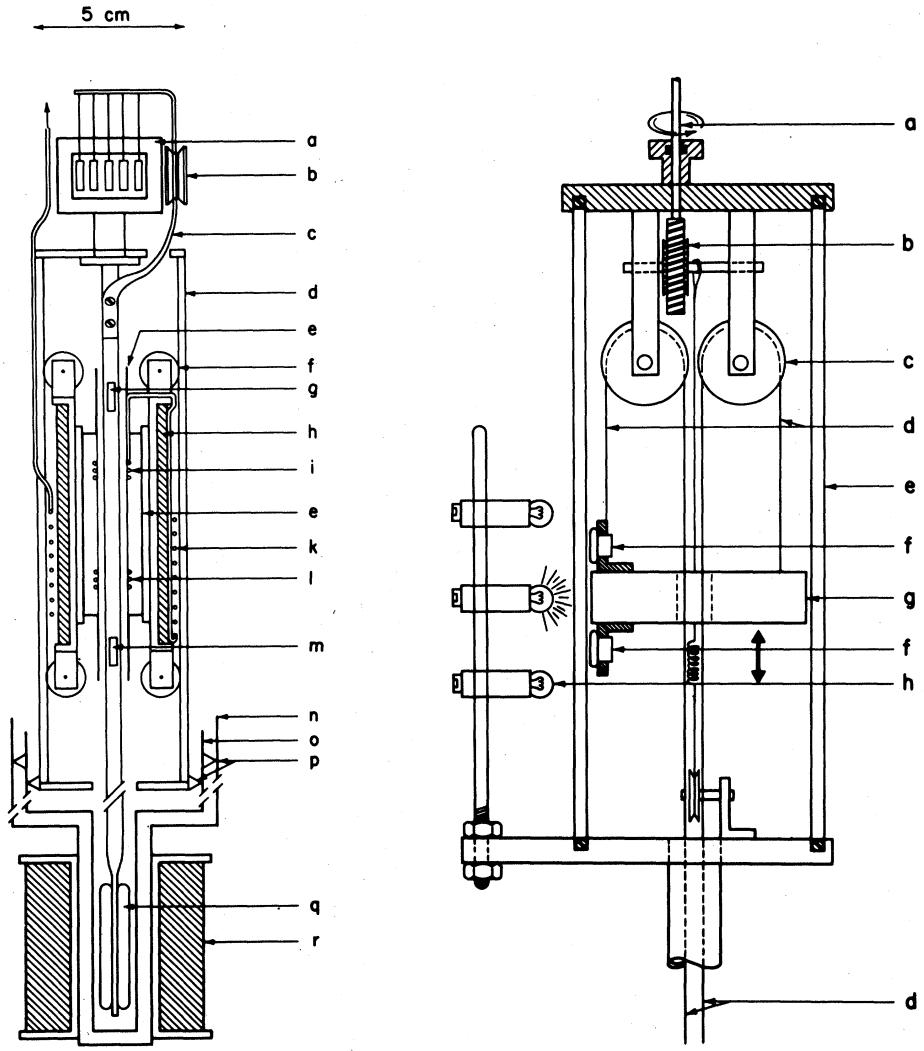

FIG. 2. Left: Very low temperature moving-coil magnetometer. (a) Mixing chamber of dilution refrigerator, (b) superconducting heat switch, (c) copper coldfinger, (d) support cage, (e) indium shield, (f) guiding rollers, (g) upper sample, (h) field coil, (i) upper SQUID pickup coils, (k) coiled lead capillary containing SQUID lead, (l) lower SQUID pickup coils, (m) lower sample, (n) vacuum can, (o) 1 K shield, (p) spacers, (q) $PrNi_5$ cooling rods, and (r) SC solenoid. Right: Optomechanical positioning system of the moving coils, mounted on the top of the cryostat. (a) Flexible motor drive rod, (b) worm gear, (c) suspension wheels, (d) silk threads, (e) glass cylinder, (f) differentially connected photocells, used to steer the dc motor, (g) counterweight to moving coils in cryostat, and (h) light bulbs.

mechanical mechanism which allows the coil to automatically home in on the three positions which can be set by positioning the three light bulbs. In operation, the coils are thermally anchored to the continuous heat exchanger and cool to about 0.4 K. During motion, they warm up to about 0.8 K. The warmup effect on the coldfinger is much smaller, typically 1 mK at 20 mK. Thermal contact to the samples was made by a thin layer of Apiezon grease, and temperatures were measured with thin layer Speer carbon resistors. These were calibrated against the susceptibility of cerium magnesium nitrate down to 20 mK, and by means of a $Co^{60}Co$ single-crystal nuclear orientation thermometer at lower temperatures.

III. RESULTS

The absolute volume susceptibility between 1.1 and 4.2 K of all nonmetallic samples investigated is shown in Fig. 3. The sample of pure silicon was cut from a high-purity single crystal with a reported residual concentration of ionizable impurities of less than $10^{13}/cm^3$. Its diamagnetic susceptibility is practically

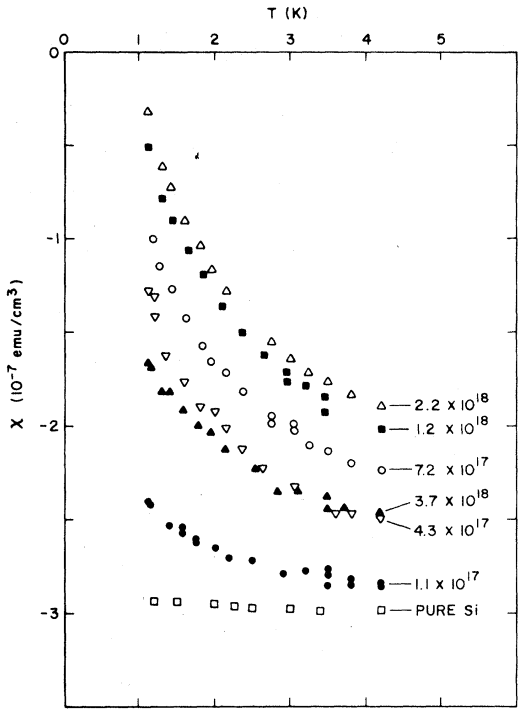

FIG. 3. Absolute volume susceptibilities between 1.1 and 4.2 K of Si:P samples with various phosphorus concentrations as indicated.

temperature independent below 4.2 K. The doped samples clearly show the paramagnetic contribution from the donor spins which increases with decreasing temperature. Although it was shown that the electrical resistivity for the highest concentration investigated here ($3.7 \times 10^{18}/\text{cm}^3$) diverges as $T \to 0$,[14] it is clear that in this sample most of the donor electrons are no longer localized around individual phosphorus ions, but those at the Fermi level are localized with a localization length which is much larger than the effective Bohr radius.

The lower-temperature donor susceptibility (χ_D) data for all insulating samples spanning the three decades of temperature between 3 mK and 4.2 K are shown in Figs. 4 and 5, where χ_D in volume units is plotted against temperature in a doubly logarithmic plot. For convenience the samples have been labeled A through E in order of increasing phosphorus concentration (see Table I). The scales for the successive concentrations are displaced by a decade for clarity, and the solid line represents the calculated Curie law for free spins at nominal concentration. The various symbols refer to different measuring fields, as indicated in the caption. The dashed lines are the results of calculations, as discussed in Secs. IV and V. It can be seen that for all concentrations, the reduction of χ_D from its free spin value increases towards lower temperatures. At 4.2 K, this reduction is only 15% for the smallest concentration ($1.1 \times 10^{17}/\text{cm}^3$), increasing to a factor of 10 at $3.7 \times 10^{17}/\text{cm}^3$. Down to about 30 mK, the temperature dependence is fairly well described by a T^{-n} law, with the exponent n varying between 0.9 for the lowest and 0.64 for the highest concentration.

It is remarkable that for all concentrations except the lowest one the donor susceptibilities become temperature independent below about the same temperature, namely, around 10 to 20 mK. For the two highest concentrations (D and E), the χ_D curves in Fig. 5 are nearly parallel to each other, i.e., χ_D of the higher concentration (sample E) is roughly a factor of 3 lower than that of sample D over the whole temperature range. This behavior reflects the greatly increased interactions which are a precursor to the metallic phase.

At the lower concentrations, we observe χ_D to become field dependent at low temperatures. For free spins, the effect of paramagnetic saturation in 50 Oe should reduce the initial susceptibility by 4% and 13% at 10 and 5 mK, respectively. An effect of this order is observed in sample C, where we would in fact not expect it, since the theoretical analysis shows that there are only few spins in this sample coupled with exchange interactions less than the equivalent of 10 mK. Even more startling field effects are seen in the lower concentration samples A and B. In sample A, the reduction of χ_D on increasing the field from 10 to 50 Oe is about a factor of 2, much larger than can be accounted for by the paramagnetic saturation effect. In sample B, a reverse field effect is observed. In 10 Oe, χ_D is flat below 20 mK, while in 50 Oe, a shallow maximum is observed around 10 mK.

The latter effect may be a consequence of unusually long spin-lattice relaxation times associated with sample B. In samples C–E the response time was typically about 2 min when warming from 3 to 5 mK, and about 5 min for sample A. In sample B, however, this response time was more than 10 min, even between 5 and 10 mK. This behavior, together with the fact that the maximum is observed only in *larger* fields, suggests that the sample was cooled into a nonequilibrium state, out of which it relaxes during the slow warmup. Similar behavior has been observed in spin-glasses, where the magnetization in the frozen state is also the higher, the slower the sample is cooled through the spin-glass freezing temperature. In our apparatus, data below 15 mK can unfortunately only be obtained while warming up, since the SQUID system is inoperative during the demagnetization cycle. During this cycle the samples are cooled in their respective measuring fields from 20 to 2 mK in a time of ~20 min (and from 10 to 2 mK in ~7 min).

One would expect the spin-lattice relaxation times to be longest in the least concentrated sample (sample A). The fact that the observed thermal relaxation

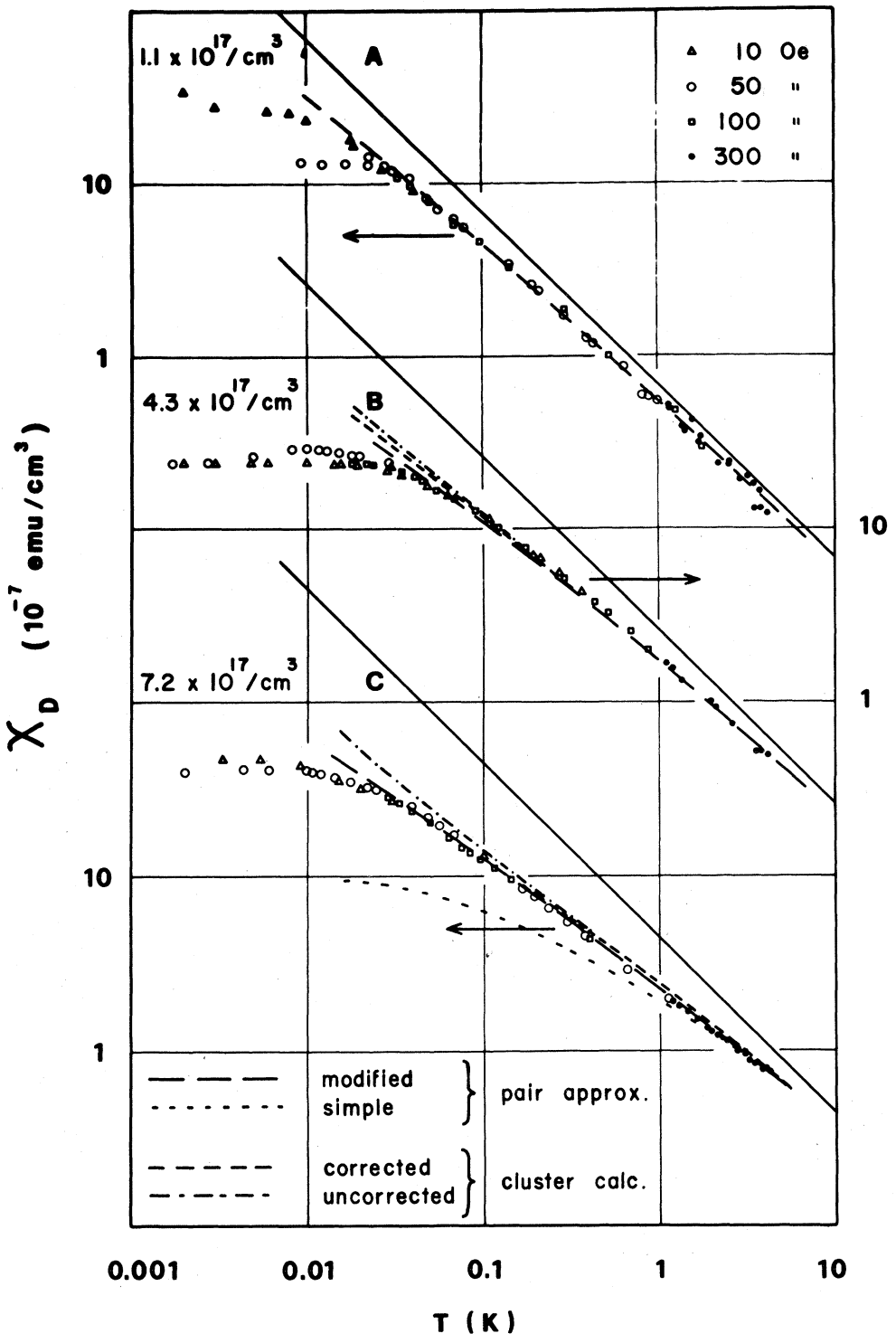

FIG. 4. Observed donor susceptibilities per unit volume in Si:P samples between 3 mK and 4.2 K in various magnetic fields, as indicated. The theoretically calculated susceptibilities are shown by various lines, as explained in the figure. Where they merge together, only the modified pair approximation (long dashes) is shown.

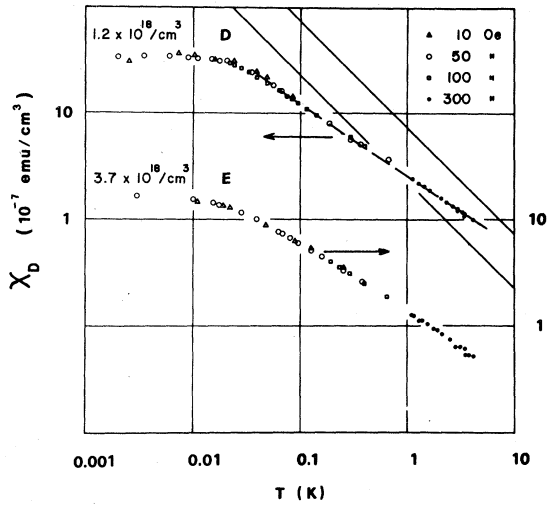

FIG. 5. Observed donor susceptibilities per unit volume in Si:P samples between 3 mK and 4.2 K in various magnetic fields, as indicated. The solid lines indicate free spin susceptibilities for these samples. The dashed line for case D is the modified pair approximation.

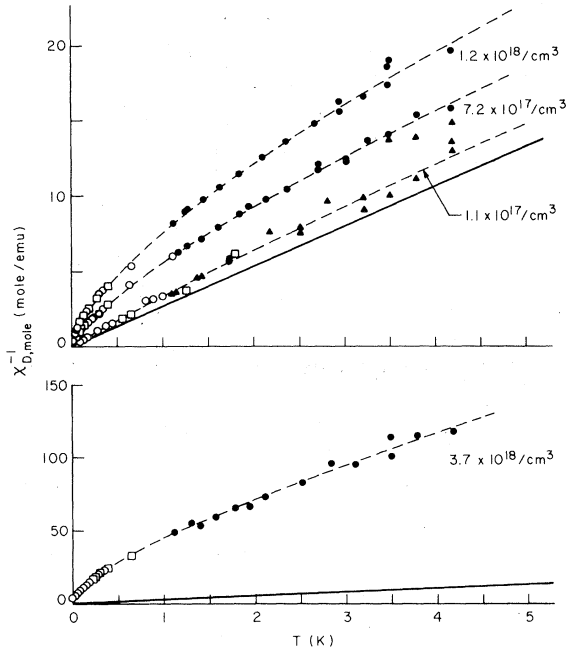

FIG. 6. Curie-Weiss plots of the molar donor susceptibilities (χ_D per mole of phosphorus ions) for the several concentrations of phosphorus in silicon investigated. Data symbols correspond to different measuring fields, as in Fig. 5. The solid line shows free spin behavior.

time of sample A below 10 mK in 10 Oe is shorter than that of sample B raises the possibility that the latter sample was "purer" in the sense that it contained a smaller concentration of magnetic impurities. This is indeed possible, since sample B originates from a different source than samples A and C (see Table I). It is also possible, then, that the observed strong field dependence of χ_D below 10 mK in sample A is in fact not an "intrinsic" property, but an effect induced by the presence of magnetic impurities.

It is also of interest to display the χ_D data in Curie-Weiss plots. This is shown in Fig. 6, where the straight line again refers to free spin behavior. True Curie-Weiss behavior, i.e., $\chi_D = C/(T+\theta)$, where $\theta(>0)$ is the arithmetic average of all exchange couplings expressed in degrees kelvin,[17] is expected only for $T > \theta$. It can be seen that even for our lowest concentration ($1.1 \times 10^{17}/\text{cm}^3$), we do not yet get into this regime at 4.2 K; i.e., there is a relevant fraction of donor pairs coupled with exchange interactions stronger than the equivalent of 4.2 K. Since we argued above that there must also be a large fraction coupled with less than 6 mK, the range of relevant exchange interactions in this sample must extend over at least four decades. This is in agreement with theoretical predictions (see Sec. IV). The characteristic downward curvature observed in all Curie-Weiss plots in Fig. 6 is another consequence of the broad distribution of interaction strengths.[9]

IV. THEORETICAL CALCULATION OF THE MAGNETIC SUSCEPTIBILITY IN THE INSULATING PHASE AND COMPARISON WITH EXPERIMENT

A. Donor wave function

In the limit of low donor concentration, the donor electrons in Si:P are well characterized by hydrogenic orbits and described by effective mass theory[15] with modifications due to the short-range part of the impurity potential, referred to as "central cell correction." In effective mass theory there are six degenerate states arising from the six conduction band valleys along the [100] directions in silicon:

$$\psi_\mu^{1s}(\vec{r}) = F_\mu(\vec{r})\phi_\mu(\vec{r}) \ , \tag{4.1}$$

where $\phi_\mu(\vec{r})$ is the Bloch wave function of the μth conduction band minimum ($\mu = \pm x, \pm y, \pm z$). $F_\mu(r)$ is the $1s$ hydrogenic envelope function well represented by the Kohn-Luttinger[15] variational form

$$F_{\pm z}(\vec{r}) = \frac{1}{(\pi a^2 b)^{1/2}} \exp\left[-\left[\frac{x^2}{a^2}+\frac{y^2}{a^2}+\frac{z^2}{b^2}\right]^{1/2}\right] , \tag{4.2}$$

with suitable permutations for the x and y valleys. (The anisotropy of the envelope function is a consequence of the anisotropy of the conduction band minima.)

The effect of the central cell in Si:P is to remove the degeneracy so that the ground state is the nondegenerate symmetric combination

$$\psi_g(\vec{r}) = \frac{1}{\sqrt{6}} \sum_{\mu} \psi_{\mu}^{1s}(\vec{r}) \quad . \tag{4.3}$$

In addition, the attractive potential in the central cell causes a shrinkage of the envelope wave function, which may be represented by a reduction in the Bohr radii a and b, estimated to be about 20%.[3]

Though there are some differences from the usual hydrogenic problem because of the anisotropy of the wave function, the isotropic (or spherical) approximation is often found to be quite reasonable, especially for the ground state, which is a symmetric combination of the six valleys, and has cubic symmetry. One then obtains an effective Bohr radius, a^*, which for Si:P is between 16–18 Å depending on the average one takes, and a corresponding Rydberg, which is close to, but somewhat less than the ionization energy, 45.5 meV. (Note that the "Bohr radius" here is enhanced relative to hydrogen by the ratio ϵ/m^*, where $\epsilon = 11.4$ is the dielectric constant and m^* an average conduction band mass, while the Rydberg is reduced by a factor ϵ^2/m^*.) Because the Bohr radius is much bigger than the Si lattice constant, the substitutional positioning of the P atoms, leading to discrete impurity sites, is not of importance.

Optical studies[3] show that for the densities below $n_D \sim 10^{17}$ cm^{-3}, the modification of the low-lying ($1s \rightarrow 2p$) excited states can be understood in terms of randomly distributed close donor pairs. For the $1s$ states (as monitored by the "forbidden" transition between the symmetric and other $1s$ states) the pair approximation works well up to $n_D \sim 10^{18}$ cm^{-3}, as expected because the radius of the $1s$ state is smaller than the $2p$ state by a factor of ~ 2. Consequently, for densities below $n_D \lesssim 10^{18}$ cm^{-3} one has a system of localized electronic spins coupled antiferromagnetically (as in the case of hydrogen) with each other. The exchange constant is determined by the splitting of the singlet and triplet state of a pair of donors.

B. Exchange interaction

The magnetic properties of isolated "monovalent" systems (such as phosphorus in silicon) are described by the spin-$\frac{1}{2}$ Heisenberg Hamiltonian

$$\mathcal{H} = \sum_{i<j} J_{ij} \vec{s}_i \cdot \vec{s}_j + \sum_i \vec{\mu}_i \cdot \vec{H} \quad , \tag{4.4}$$

where $J_{ij} = J(\vec{R}_{ij})$ is the exchange coupling between the ith and jth spins, $\vec{\mu}_i = g\mu_B \vec{s}_i$ is the magnetic moment of the ith spin and $\vec{H}$ the external field. ($g \simeq 2$ is the gyromagnetic ratio and μ_B the Bohr magneton.) We have used the convention of a positive sign in the first term on the right of Eq. (4.4), which corresponds to positive exchanges for antiferromagnetic coupling. This is convenient in the present context, as it obviates the necessity of putting negative signs all over in the text, which could cause confusion. Magnetic dipolar interactions between donor moments are estimated to be $\sim 10^{-6}$ K and have therefore been neglected.

An *ab initio* calculation of the exchange coupling for a pair of phosphrus donors in silicon, taking into account the wave function anisotropy, central cell effects, and the wave function distortion due to the presence of the other donor is not available. However, assuming that the orbital part of the ground-state pair wave function can be represented as a product of one-electron wave functions of proper symmetry and restricting oneself to the valley-symmetric combination forced by the central cell potential, the exchange coupling can be written as (see Appendix A)

$$J(\vec{R}) = \frac{1}{36} \sum_{\mu\nu} \cos(\vec{k}_\mu \cdot \vec{R}) \cos(\vec{k}_\nu \cdot \vec{R}) j_{\mu\nu}(\vec{R}) \quad , \tag{4.5}$$

where $\vec{k}_\mu$ and $\vec{k}_\nu$ are the wave vectors of the conduction band minima, and $j_{\mu\nu}(\vec{R})$ is an exchange integral involving the envelope functions for electrons in the μth and νth valley [Eq. (A4)]. The result is an exchange coupling which oscillates rapidly on the scale of the Bohr radius (with a period of the order of the lattice constant). The oscillations are due to the mismatch of the phase of the Bloch wave part of the electron wave function at the two donor sites. They are a direct consequence of the central cell potential. For the present we shall neglect the anisotropy of the envelope functions; the effect of the anisotropy will be examined in detail in the next subsection. Equation (4.5) then reduces to

$$J(\vec{R}) = \left[\frac{1}{6} \sum_{\mu} \cos(\vec{k}_\mu \cdot \vec{R}) \right]^2 j_s(R) \quad , \tag{4.6}$$

where $j_s(R)$ is the hydrogenic value. The latter has been calculated in detail by Kolos and Wolniewicz[4] for $R \lesssim 10 a_B$, and their results match well to the asymptotic ($R \rightarrow \infty$) expression derived by Herring and Flicker[5]

$$j_s(R) \approx 1.636 \left(\frac{R}{a_B} \right)^{5/2} e^{-2R/a_B} \quad (R \rightarrow \infty) \quad . \tag{4.7}$$

The simplest approximation to treat the rapidly oscillating factor in Eq. (4.6) is to average it, which leads to a hydrogenic exchange reduced by the factor 6. However, a better approximation, which we have chosen to employ, is to treat $J(\vec{R})$ as $j_s(R)$ multiplied by a random variable ϕ which varies between 0 and 1 with the appropriate probability distribution.

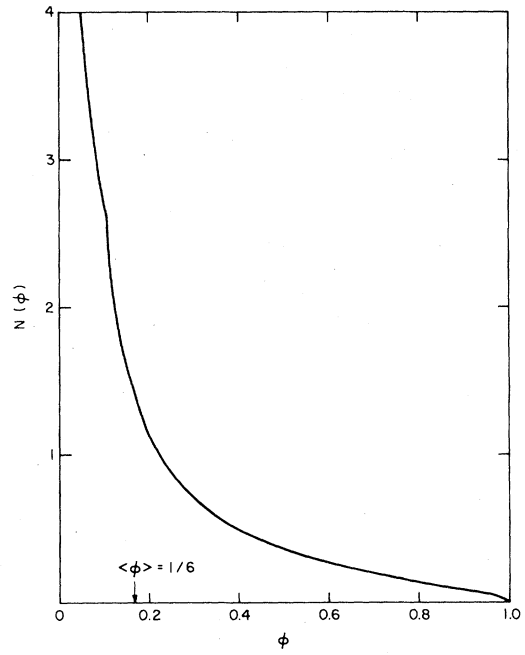

FIG. 7. Plot of the probability density $N(\phi)$ of the attenuation factor ϕ $(0 < \phi < 1)$ which reduces the hydrogenic exchange interaction due to phase mismatch (see text and Appendix A).

This distribution is computed in Appendix A and shown in Fig. 7. Because of the inverse-square-root singularity at the origin [Eq. (A9)], the distribution of the random variable is heavily biased towards small values. This leads to a much weaker exchange coupling than the hydrogenic case, which applies to direct gap semiconductors such as CdS.[9] The singularity also leads to a longer weak-coupling tail in the probability distribution of the nearest-neighbor exchange than expected by the simple averaging procedure. This has an effect similar to a reduction of the concentration.

C. Pair approximation

The simple pair approximation has been found to be satisfactory in explaining the magnetic susceptibility of doped semiconductors at low concentrations and high temperatures. In this approximation one simply pairs each spin with its strongest-coupled neighbor, and solves for the susceptibility of pairs of spins. For pairs and $s = \frac{1}{2}$ spins with Heisenberg exchange, one easily obtains

$$\chi_p(T) = \chi_c(T) \int_0^{J_{\max}} \frac{4p(J)\,dJ}{3 + e^{J/T}} \quad , \tag{4.8}$$

where

$$\chi_c(T) = \frac{n_D \mu_B^2}{k_B T} \tag{4.9}$$

is the Curie susceptibility for free $s = \frac{1}{2}$ spins with $g = 2$. (Here n_D is the donor density, μ_B the Bohr magneton, k_B the Bolzmann constant, and T the temperature.) J is the singlet-triplet splitting and $p(J)$ the probability distribution of the exchange couplings of the strongest-coupled neighbor.

For a single valley isotropic semiconductor the exchange splitting J is a function only of the magnitude of the separation (R) of the spins in the pair, and monotonically decreases with increasing R. $p(J)$ is easily obtained from the nearest-neighbor probability distribution from randomly positioned donors $[P_{\rm NN}(R)]$

$$p(J) = \left| \frac{P_{\rm NN}(R)}{dJ/dR} \right|_{J(R)=J} \quad , \tag{4.10}$$

where

$$P_{\rm NN}(R) = 4\pi n_D R^2 \exp(-\tfrac{4}{3}\pi n_D R^3) \quad . \tag{4.11}$$

However, in Si:P, the exchange interaction is not spherically symmetric and is multiplied by a rapidly oscillating phase factor. The formulas [(4.10) and (4.11)] require appropriate generalization.

First we consider the effect of anisotropy, and compare the results for the anisotropic and isotropic interactions. In this comparison we set aside the complications due to the random phase factor and simply use the average value. Thus we obtain

$$J(\vec{R}) = \tfrac{1}{18}[j_{xx}(\vec{R}) + j_{yy}(\vec{R}) + j_{zz}(\vec{R})] \quad . \tag{4.12}$$

The $j_{\mu\mu}(\vec{R})$ are evaluated in Appendix B within the Heitler-London approximation using Kohn-Luttinger wave functions [Eq. (4.2)]. We note that the Heitler-London results for hydrogen differ significantly from those of Kolos and Wolniewicz. However, the effect of anisotropy should be similar for both forms.

The probability density of having a nearest-neighbor exchange is then given by

$$p(J) = n_D \rho(J) \exp\left[-n_D \int_J^{J_{\max}} \rho(J')\,dJ'\right] \quad , \tag{4.13}$$

where $\rho(J)$ is the density of J values

$$\rho(J) = \int \delta(J - J(\vec{R}))\,d^3R \quad .$$

Using the appropriate Kohn-Luttinger radius ratio $a/b = 1.73$ we obtain the plots of $p(J)$ shown in Fig. 8, for two values of the dimensionless density $n_D a^2 b = 0.0005$ and 0.003. [Because of the large range of exchange couplings, we use $\ln J$ as the variable, with a probability density $p(\ln J)\,d\ln J \equiv p(J)\,dJ$,

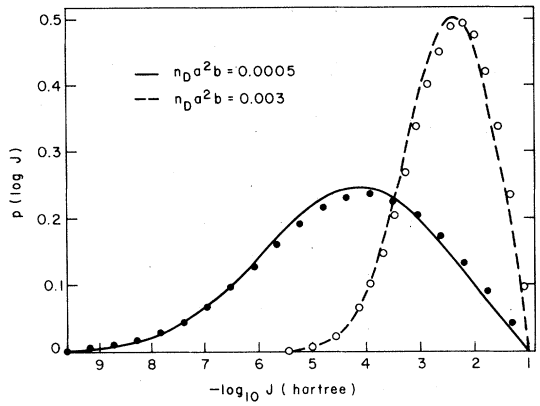

FIG. 8. Distribution of nearest-neighbor exchange couplings $p(\ln J)$ for isotropic (circles and points) and anisotropic exchange interactions (appropriate for Si:P, dashed and solid lines) for two values of $n_D a^2 b$, as indicated. *In this figure,* calculations have been done using the Heitler-London approximation and the average value of the attenuation factor.

or $p(\ln J) = Jp(J)$.] The results for the isotropic interaction ($a/b = 1$) with an effective radius a^* [$a^* \simeq 1.07(a^2 b)^{1/3}$ for $n_D a^2 b = 0.0005$ and $a^* \simeq 1.03(a^2 b)^{1/3}$ for $n_D a^2 b = 0.003$] are shown as points. The values of a^* were adjusted to obtain the best fit. Still better agreement can be obtained by adjusting the energy scale (Rydberg) somewhat, but since our results for susceptibility are least sensitive to small changes in the Rydberg, we have chosen not to do so. The results calculated for the isotropic interaction are within a few percent of the $p(J)$ obtained for the anisotropic interaction. Consequently, in subsequent work we will use the approximation of an isotropic interaction. The slight variation in a^* reflects the fact that for lower concentrations one is way down in the exponential tail of $J(\vec{R})$, where the coupling is dominated by the largest radius. This gives a slightly larger effective isotropic radius than the mean value appropriate at higher concentrations. This trend is also found in our values fitted to the experimental results.

Having demonstrated that the exchange coupling for the symmetric ground state can be adequately represented by an isotropic $J(R)$, we use the expression derived in the last section:

$$J(R) = \phi j_s(R) \ ,$$

where ϕ varies between 0 and 1. The probability density of ϕ, $N(\phi)$ is given in Appendix A and shown in Fig. 7. This leads to the result that $J(R)$ is not a monotonically decreasing function of R, and that the nearest neighbor may not be the strongest magnetically coupled neighbor. The distribution of exchange couplings for the *strongest* magnetically coupled neighbor, as generalized from Eq. (4.13) is shown in Appendix C to be

$$p(J) = \int_0^{R_H(J)} 4\pi n_D R^2 dR j_s(R)^{-1} N\left(\frac{J}{j_s(R)}\right) \times \exp\left[-\int_0^{R_H(J)} 4\pi n_D R'^2 dR' \int_{J/j_s(R')}^1 N(\phi) d\phi\right] , \tag{4.14}$$

where R_H is the radius at which the hydrogenic exchange equals J; i.e.,

$$j_s(R_H) = J \ . \tag{4.15}$$

The distribution of exchange couplings for the nearest neighbor $\tilde{p}(J)$, on the other hand is (see Appendix C):

$$\tilde{p}(J) = \int_0^{R_H(J)} 4\pi n_D R^2 dR e^{-(4\pi/3) n_D R^3} j_s(R)^{-1} N\left(\frac{J}{j_s(R)}\right) . \tag{4.16}$$

Figure 9 shows the difference in the distribution of couplings for the strongest coupled and nearest neighbor for a typical concentration ($\sim 8 \times 10^{17}$ cm^{-3} in Si:P), along with the distribution for hydrogenic exchange. The curves were calculated with the Kolos-Wolniewicz-Herring-Flicker (KWHF) values

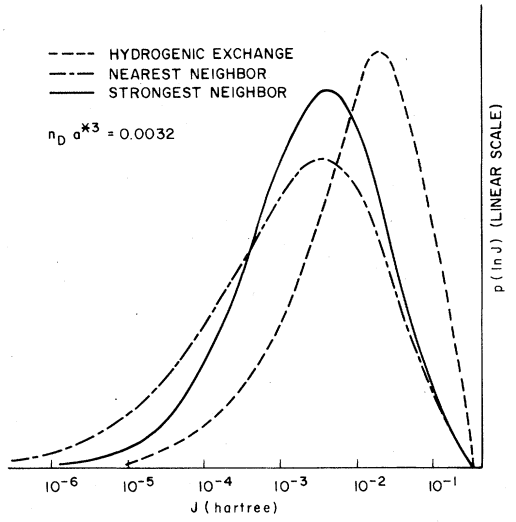

FIG. 9. Calculated probability densities $p(\ln J)$ for hydrogenic exchange (dashed line, valid for direct-bandgap, single-valley semiconductors) and for the multivalley case of silicon, both for nearest neighbor (dash-dotted line) and for strongest neighbor (solid line) exchange. These results are calculated with KWHF exchange, using spherical envelope functions.

for $j_s(R)$ in Eqs. (4.14), (4.16), and (4.10). As emphasized earlier, the exchange is reduced by about an order of magnitude from the hydrogenic case. In addition, Fig. 9 clearly shows that the fluctuations of the phase factor lead to rather different distributions for the nearest neighbors and the magnetically strongest coupled neighbors.

D. Modified pair approximation

The pair approximation works well at high temperatures and low concentrations. In this limit, the only spins "frozen" out are those which are unusually close, and because of the exponential form of the interaction, these are very likely to be isolated pairs. However, as has been shown,[11] even for low concentrations it breaks down at low temperatures, when the susceptibility drops below about 70% of the Curie value. Numerous remedies have been suggested, including grouping spins into sets of three,[7] and modifying the nearest-neighbor distribution to take into account the possibility that the neighbor is already "paired up" with another spin.[16] The former forces a doublet ground state for each set of three spins, thus leading to a significantly overestimated susceptibility, equal to one-third the Curie value, at low temperatures. The latter treats the probability distributions for the neighbors of the spins in the pair as independent, which again can be shown to overestimate the susceptibility. We present in this section another method of improving on the pair approximation, which correctly takes into account three spin clusters, and also we believe gives a good approximation to the behavior of larger ones. The method has been found[11] to give results within $\approx 10\%$ of numerical cluster methods down to temperatures where the susceptibility is 20% of the Curie value. Further improvement should be possible by studying the statistics of the energy levels of finite sized larger clusters.

The procedure starts with a calculation of the susceptibility in the simple pair approximation. Using the KWHF exchange, Eqs. (4.14) and (4.8), we compute the susceptibility in the simple pair approximation. The temperature-dependent ratio

$$f(T) \equiv \chi_p(T)/\chi_c(T) \tag{4.17}$$

gives the fraction of effectively isolated spins at a temperature T (i.e., those with strongest couplings $J \lesssim k_B T$). This naturally leads one to define an effective, temperature-dependent, clustering volume through

$$f(T) \equiv \exp[-n_D v(T)] \ . \tag{4.18}$$

[Equation (4.18) is motivated by the result that the probability of finding no neighbors in a volume v around a given spin at a density n_D is $\exp(-n_D v)$.]

To evaluate the contribution of each spin to the susceptibility at a temperature T, we imagine circumscribing a volume $v(T)$ around the spin. We allow for the possibility of all numbers of spins n in v given by the Poisson distribution, and ascribe to each spin $1/n$ of the susceptibility of the n-spin cluster.[17] Since the spins in the cell are connected to each other by bonds of order T or greater, we expect only the ground state to be relevant at T. All even numbered clusters are assumed to have a singlet ground state (all spins paired) while odd numbered clusters have a doublet ground state (one spin free). This leads to a susceptibility in this modified pair approximation:

$$\begin{aligned}\chi_{\mathrm{MPA}}(T) &= \chi_c(T) e^{-n_D v}\left[1 + \frac{1}{3}\frac{(n_D v)^2}{2!} + \frac{1}{5}\frac{(n_D v)^4}{4!} + \cdots\right] \\ &= \chi_c(T) e^{-n_D v} \sinh(n_D v)/(n_D v) \ . \end{aligned} \tag{4.19}$$

Using Eqs. (4.17)–(4.19) one easily obtains

$$\frac{\chi_{\mathrm{MPA}}(T)}{\chi_c(T)} = \frac{1 - [\chi_p(T)/\chi_c(T)]^2}{2\ln[\chi_c(T)/\chi_p(T)]} \ , \tag{4.20}$$

which reduces to the simple pair approximation at high temperatures when few spins are frozen out. In this limit $\chi_p/\chi_c \to 1$ and

$$\chi_{\mathrm{MPA}}(T) \approx \chi_p(T)\left[1 + \tfrac{1}{6}\left[1 - \frac{\chi_p(T)}{\chi_c(T)}\right]^2 + \cdots\right] \ . \tag{4.21}$$

Alternatively one can arrive at Eq. (4.19) by dividing the system into cells of volume v and evaluating the susceptibility of each cell independently, allowing for a Poisson distribution of spins in each cell.

Using Eq. (4.20) we obtain the susceptibility curves shown in Figs. 4 and 5 as the long dash lines. Both donor concentration n_D and the effective Bohr radius a^* have been adjusted to give a good fit, with the resulting parameter values given in Table I. A good fit to experiment is achieved, except for the lowest temperatures, and the values of n_D obtained agree with those derived from the room-temperature resistivity data to within about 5%. This demonstrates that this method is an independent measure of concentration. A detailed comparison of these calculations with the experimental data is given in Sec. V, along with a discussion of the fitted parameters.

It is interesting to examine the low-temperature limit of $\chi_{\mathrm{MPA}}(T)$. In this limit $\chi_p(T) \to 0$, leading to

$$\chi_{\mathrm{MPA}}(T) \approx \frac{\chi_c(T)}{2\ln[\chi_c(T)/\chi_p(T)]} \quad (T \to 0) \ . \tag{4.22}$$

For exponential interactions this gives a diverging

susceptibility $\chi_{\mathrm{MPA}}(T \to 0) \sim [T \ln^3(T_0/T)]^{-1}$, in marked contrast with the pair approximation. Applying the same argument for power-law couplings $J(R) \sim R^{-n}$ gives divergent susceptibility (and thus no spin-glass behavior) for $n > 3$; this value for the crossover has been arrived at by Fisch[18] using a different approach.

A comparison of the results obtained by the present method with the more detailed cluster calculation to be described in the next section shows this to be an accurate and useful approximation to $\chi(T)$ down to the lowest temperatures where the cluster calculations are valid. However, at lower temperatures the validity of our procedure of replacing the infinite system by an ensemble average of finite clusters in a temperature-dependent volume is an open question. Assessment of this point awaits a more rigorous theory. If our scheme is found to be justified, it would be of great interest to do statistics on the energy levels of larger clusters (in the way we have defined them) and incorporate their low-lying excited states to improve our approximation.

E. Cluster analysis of computer simulation

The Si:P susceptibility data have also been analyzed by a computer simulation technique which has been applied successfully to the case of dilute donors in CdS.[9] We give here a brief sketch of this method of analysis, a more detailed description being found in Ref. 9. Random sites in a cubic volume are selected for a finite sample of N spins. The exchange interaction matrix is then set up using Eq. (4.4). The interference factor in Eq. (4.6), which was absent in the CdS case, is treated as a random statistical variable because of its rapid variation with $\vec{R}$. The value of this factor for a given exchange bond is determined by choosing a random number on the unit interval, these numbers being distributed as given in Appendix A. The exchange interaction is limited to a range of $R \leq 9a_B$, giving $J(\vec{R})$ values ranging over more than five orders of magnitude. Periodic boundary conditions are applied to the simulation cube to avoid surface effects.

The magnetic properties of the simulated spin system described are calculated with the following approximate scheme. The system is divided into clusters by setting an interaction threshold Δ such that if $J_{ij} > \Delta$, then spins i and j are in the same cluster. Δ is set at or near the minimum temperature of the data to be analyzed, if possible. The cluster Hamiltonians are solved exactly and the magnetization of the entire system is then calculated, taking intercluster interaction into account with a molecular field scheme. Thus, the system Hamiltonian [Eq. (4.4)] is approximated by one which is a sum over clusters n, $\mathcal{H}_{\mathrm{app}} = \sum_n \mathcal{H}_n$, where

$$\mathcal{H}_n = -g\mu_B(H + h_n)\sum_i{}' S_{zi} + \tfrac{1}{2}\sum_{i\neq j}{}' J_{ij}\vec{S}_i \cdot \vec{S}_j \ , \quad (4.23)$$

where $\sum'$ indicates a sum over the nth cluster and

$$h_n = (2g\mu_B N_n)^{-1}\langle\sigma_z\rangle_{\mathrm{av}} \sum_{jk}{}'' J_{jk} \quad (4.24)$$

is the molecular field acting on that cluster. In Eq. (4.24) the sum $\sum''_{jk}$ is over spins j in cluster n and k not in cluster n. N_n is the number of spins in cluster n and $\langle\sigma_z\rangle_{\mathrm{av}}$ is the mean polarization ($0 \leq \langle\sigma_z\rangle_{\mathrm{av}} \leq 1$) for the entire sample. There is a practical limit on the size of clusters to be diagonalized, which we have set at eight. Larger clusters are broken down into smaller units by cutting the weakest bonds possible and/or eliminating strongly coupled spin pairs which are sufficiently isolated to remain magnetically inert.

This method is exact in the limit of low concentrations and high temperatures. As these conditions are relaxed, we estimate the accuracy of the results by the size of the molecular field corrections. Although these corrections are probably no more accurate than within a factor of 2, when they are small the results are thought to be correspondingly precise. While the simulation method gives no analytic results, it is useful both to compare with data and to test the analytic results of Secs. IV C and IV D under conditions where the accuracy is good.

The qualitative nature of the results reported here are quite similar to those obtained earlier for CdS,[9] in spite of the topologically different clusters which result from a nonmonotonic dependence of the exchange interaction on separation. The magnetic contribution from each cluster at temperature T is obtained by weighting the Curie constants from the various spin multiplet eigenstates according to their degeneracy and Boltzmann factor. Since the states with lower spin tend to lie lower in energy, one finds an overall Curie constant that diminishes steadily toward low temperatures. All odd clusters are found to possess doublet ground states, whereas a significant fraction of even cluster ground states are triplets (the remainder being singlets). Eight-spin clusters contribute, for example, the same susceptibility per spin as all clusters do on the average. We emphasize that clusters as defined here and in the modified pair approximation are totally different; thus, there is no simple relationship between the results obtained with these two methods.

Cluster analyses of two independent random distributions of $N = 324$ spins have been carried out for each of the three lowest concentrations (Fig. 4) using the parameter values given in Table I. The two calculated susceptibility curves at each concentration differed by a few percent at most; averages of the two are plotted in Fig. 4 both with (short dash line) and

without (dot-dash line) molecular field corrections. In cases where the corrected cluster analysis curve is indistinguishable from the modified pair approximation result (Sec. IV D) the short dash line is omitted. In fact, the latter condition applies everywhere except in the vicinity of 1 K for sample C and below ~ 100 mK for sample B. For sample A the molecular field corrections are negligible down to 10 mK, thus the "uncorrected" curve is omitted.

The correspondence between these results and both the modified pair approximation curves and the experimental data are discussed in detail in the next section.

V. DISCUSSION AND CONCLUSIONS

This work has measured the magnetic susceptibility of phosphorus doped silicon in the temperature range 4 K down to 2 mK, for doping levels n_D ranging from just below the delocalization transition at $\sim 4 \times 10^{18}$ cm^{-3} down to 10^{17} cm^{-3}. To our knowledge, this is the most thorough investigation to date of an $s = \frac{1}{2}$ amorphous system with antiferromagnetic Heisenberg exchange over temperatures ranging to well below the magnetic percolation threshold of the system.

Down to about 25 mK, the donor susceptibility is found to be a monotonically increasing function as the temperature is reduced. However, the slope on a log-log plot of susceptibility versus temperature is much reduced from the Curie law (slope equal to -1), and the susceptibility at low temperatures is extremely nonlinear in donor concentration in the above range. The data are not fitted by a Curie-Weiss form, because the exchange couplings range to well above the temperatures studied. For concentrations $n_D \lesssim 1 \times 10^{18}$ cm^{-3} and $T \gtrsim 30$ mK, the modified pair approximation and numerical cluster calculation using the same *a priori* values of the exchange interaction are in agreement with each other. Both are found to give excellent agreement with experiment as shown in Fig. 4. Note that at the lower temperatures in this range, the susceptibility is much less than the Curie value. The only parameters which enter these calculations are the donor concentration n_D, the effective Bohr radius a^*, and the effective rydberg, $\mathfrak{R}$. The fits are not sensitive to the values of $\mathfrak{R}$ and we have used an average value $\mathfrak{R} = 440$ K for all concentrations. This value falls within the range defined by $\mathfrak{R} = e^2/2\epsilon a^*$. The values of n_D and a^* are quoted in Table I. They are found to be within a few percent of the values obtained from other measurements.[3] This confirms the basic correctness of our model. The decrease in a^* with n_D is small, and of the magnitude that is expected because of the approximation of the anisotropic envelope functions by isotropic ones. The agreement of better than 5% in n_D with values derived from conductivity shows that the susceptibility can be used as an independent reliable measure of concentration.

In Fig. 10 we show the donor susceptibility versus concentration at two fixed temperatures. The increase in strength of exchange interactions as n_D is increased causes χ_D to deviate from the Curie susceptibility, which is linear in n_D. As expected, the departure from linearity is more pronounced at the lower temperature. Also shown are values of χ_D obtained in the modified pair approximation, which agree well up to concentrations $n_D \sim 1.2 \times 10^{18}$ cm^{-3} (see also Fig. 5). That the fit is good up to these concentrations may appear somewhat surprising. The implied absence of a change in the exchange interaction indicates that extensive delocalization takes place only at higher densities, i.e., within a factor of 4 of the Mott density. (We note in passing that the transition from the metallic side has been found to be very abrupt in recent low-temperature conductivity studies.[19]) At still higher concentrations, the accuracy of both types of calculation is expected to deteriorate.

At the lowest temperatures, there is a systematic deviation of the experimentally measured susceptibility from the calculated results, toward lower values. In samples A, C, and D the deviation is rather abrupt and takes place at $T \sim 30$ mK, independent of n_D. The concentration independence suggests that the deviation is not likely to be caused by ordering of the electronic spins due to their mutual interactions (exchange or dipolar). Other causes for the saturation could include nonequilibrium effects, or possibly other interactions such as those between electronic and nuclear spins (hyperfine) or with other impurities, etc., which have not been included in the Hamiltonian. We have examined the possibility of susceptibility saturation due to hyperfine condensation (the hyperfine interaction in Si:P is about 5 mK) by calculat-

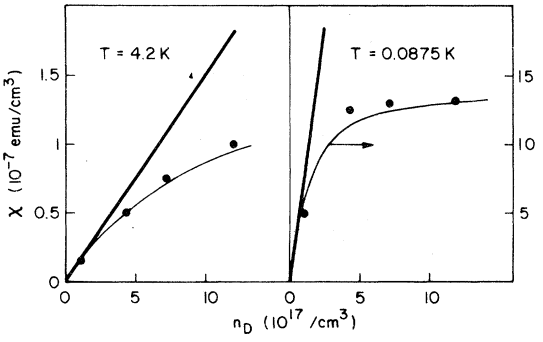

FIG. 10. Observed donor susceptibilities as a function of donor concentration at 4.2 and 0.0875 K (solid circles). Also shown are the values for free spins (heavy solid lines) as well as those calculated in the modified pair approximation (light solid lines).

ing the susceptibility of clusters of one, three, and (magnetic) four electronic spin clusters. The hyperfine interaction in dilute Si:P is about 5 mK. The deviations obtained at $T \sim 10-20$ mK, however, are not adequate to explain the discrepancy between theory and experiment. Regarding other possibilities, it is difficult to rule out nonequilibrium effects in the experiments as a cause of the observed saturation, although the equilibrium appeared to be good at temperatures of 20 mK and above. The variation of the saturation effect among samples A–C suggests that it is nonintrinsic behavior caused by magnetic impurity species.

Particularly anomalous behavior of the susceptibility is seen for sample B which was obtained from a different source from any of the other samples (Table I). First, the Bohr radius needed to fit the susceptibility (15.2 Å) is lower than expected from the fits to the other samples. At low temperature, long relaxation times of the order of 10–20 min were observed, and in the SQUID measurement the sample actually showed a small peak in susceptibility in a field of 50 Oe, which disappeared in 10 Oe. Also, the saturation effect in this sample is reversed from that for the lowest concentration sample (which has the correct sense but is anomalously large). We believe this behavior is likely to be due to nonequilibrium effects rather than spin-glass type ordering. The nonequilibrium effects seen in this sample point to the possibility of the same in other samples at temperatures below 20 mK.

The possibility that the observed saturation effect in any of the samples is actually spin-glass ordering has to be rejected because of its unexpectedly small variation with concentration. For example, in sample C the measurements extend to well below the percolation temperature for the exchange bonds.[10] Yet, if the observed flattening of χ_D below $T \sim 30$ mK were a spin-glass transition, then the corresponding transition in samples A and B would have to occur at temperatures well below 30 mK. Since they do not, we are forced to conclude that the flattening is due to some other effect which takes precedence.

In view of the absence of identifiable spin-glass transitions in our Si:P samples, it is useful to consider further the contrasting features of Si:P and typical spin-glass materials which were mentioned in Sec. I. First, no spin-glass transition has been reported in a system with spins $s = \frac{1}{2}$. Klemm[20] has argued that spin-glass transitions do not exist for such systems. Recently, however, Bray and Moore[21] have predicted such a transition for the Sherrington-Kirkpatrick model with $s = \frac{1}{2}$. A second point is the purely antiferromagnetic character of the exchange in Si:P. Although spin-glass ordering is frequently said to occur because of the competition between ferro- and antiferromagnetic bonds, recent work[22] has strongly indicated that purely antiferromagnetic systems can exhibit spin-glass behavior. Finally, a most important point is the short-range interaction in Si:P, which leads to a very wide range of nearest-neighbor interactions. In this respect Si:P resembles diluted antiferromagnets below their percolation threshold, which exhibit no magnetic transition. In contrast, spin-glasses tend to have a relatively narrow distribution of exchange couplings. What may happen in Si:P below the percolation temperature is that strongly-coupled clusters condense into singlet ground states, i.e., magnetically inert regions.[23] The system is then unable to support the long-range correlations believed to characterize the spin-glass transition.

At concentrations above $\sim 10^{18}$ cm^{-3}, but still below the insulator-metal transition, the donor electrons are not in the isolated donor orbits, and consequently the spin susceptibility cannot be described in terms of our model for the exchange interaction. Instead the description is in terms of a strongly correlated Fermi gas, with disorder-induced Anderson localization at the Fermi level. While the moderate temperature dependence of $\chi(T)$, which disappears only on the metallic side of the transition where one obtains a Pauli T-independent susceptibility, is in qualitative agreement with this picture, there exists no complete theory for this region.

It would be highly desirable to complement our results in Si:P by other experiments which are directly sensitive to nonzero expectation values of spin $\langle S_z \rangle$ at the donor sites. Examples include line broadening due to freezing of spins in EPR, or possibly nuclear orientation techniques. (One could look for anisotropy in γ radiation of neutron-activated phosphorus nuclei which orient themselves in the local hyperfine fields at low temperatures.) In the search for magnetic ordering due to the magnetic exchange interaction, the direct gap doped semiconductors with large donor binding energies offer greater promise because there is no reduction of exchange due to many-valley effects, and thus the interference due to hyperfine coupling is also not as great.

ACKNOWLEDGMENTS

The authors would like to thank S. Geschwind and G. A. Thomas for useful discussions.

APPENDIX A: EXCHANGE INTEGRAL FOR SHALLOW DONORS IN Si

The exchange energy for a pair of donors at $\vec{R}_A$ and $\vec{R}_B$ with electrons in the symmetric $1s$ ground state (with envelopes perturbed as necessary by the presence of each other) is given by

$$J(\vec{R}_B-\vec{R}_A)=\int d^3r_1 d^3r_2 \psi_g^*(\vec{r}_1-\vec{R}_A)\psi_g^*(\vec{r}_2-\vec{R}_B)\frac{e^2}{\epsilon|\vec{r}_1-\vec{r}_2|}\psi_g(\vec{r}_1-\vec{R}_B)\psi_g(\vec{r}_2-\vec{R}_A) \ , \tag{A1}$$

where

$$\psi_g(\vec{r})=\frac{1}{\sqrt{6}}\sum_\mu \tilde{F}_\mu(\vec{r})\phi_\mu(\vec{r}) \tag{A2}$$

is the ground-state wave function centered around the origin. The sum on μ is over the six conduction band minima located at $\vec{k}=\vec{k}_\mu$ with Bloch wave functions $\phi_\mu(\vec{r})\sim\exp(i\vec{k}_\mu\cdot\vec{r})$, and $\tilde{F}_\mu$ are the corresponding (anisotropic) perturbed "hydrogenic" envelopes. Substituting Eq. (A2) in Eq. (A1), and neglecting terms for which the integrand is rapidly oscillating, we obtain

$$J(\vec{R})=\frac{1}{36}\sum_{\mu,\nu} j_{\mu\nu}(\vec{R})e^{i(\vec{k}_\mu-\vec{k}_\nu)\cdot\vec{R}} \ , \tag{A3}$$

where

$$j_{\mu\nu}(\vec{R})=\int d^3r_1 d^3r_2 \tilde{F}_\mu(\vec{r}_1-\vec{R}_A)\tilde{F}_\nu(\vec{r}_2-\vec{R}_B)\frac{e^2}{\epsilon|\vec{r}_1-\vec{r}_2|}\tilde{F}_\mu(\vec{r}_1-\vec{R}_B)\tilde{F}_\nu(\vec{r}_2-\vec{R}_A) \tag{A4}$$

and $\vec{R}=\vec{R}_B-\vec{R}_A$.

The valleys at $\vec{k}_\mu$ and $-\vec{k}_\mu$ have the same envelopes leading to

$$J(\vec{R})=\frac{1}{36}\sum_{\mu\nu}\cos(\vec{k}_\mu\cdot\vec{R})\cos(\vec{k}_\nu\cdot\vec{R})j_{\mu\nu}(\vec{R}) \ . \tag{A5}$$

If we assume the envelope functions to be spherical, so $j_{\mu\nu}(\vec{R})\equiv j_s(R)$, independent of μ and ν, we immediately obtain

$$J_s(\vec{R})=\left[\frac{1}{6}\sum_\mu\cos(\vec{k}_\mu\cdot\vec{R})\right]^2 j_s(R) \ . \tag{A6}$$

On the other hand, if we average over the rapidly oscillating cosine terms, only the terms with $\mu=\pm\nu$ survive, to give

$$\langle J(\vec{R})\rangle=\frac{1}{36}\sum_\mu j_{\mu\mu}(\vec{R}) \ . \tag{A7}$$

Obviously a combination of Eqs. (A6) and (A7) leads to an averaged exchange $\langle J_s(\vec{R})\rangle$ which is spherically symmetric and equal to $j_s(R)/6$.

For the spherical case (A6) we may do better than averaging over the cosine factor, by noticing that since the lattice constant is much less than the Bohr radius, the effect of the cosine factor can be represented by a random number ϕ, between 0 and 1, multiplying $j_s(R)$. The probability density (distribution function) $N(\phi)$ of the random number ϕ is just the density of states for a band whose energy dispersion is the square of the energy dispersion for a three-dimensional simple cubic tight binding band of s states. While no analytic form exists for this distribution function we have found the following formula to be accurate within $\sim 2\%$, for the simple cubic tight binding density of states

$$D(\epsilon)=\begin{cases}\sqrt{3}/2, & |\epsilon|\leq\frac{1}{3}\\ [\frac{3}{8}(1-|\epsilon|)]^{1/2}[\sqrt{3}+(|\epsilon|-\frac{1}{3})-\frac{2}{9}\pi^2(|\epsilon|-\frac{1}{3})^{1/2}], & 1\geq|\epsilon|\geq\frac{1}{3}\end{cases} \ . \tag{A8}$$

This leads to a probability density for $\phi=\epsilon^2$ of

$$N(\phi)=\frac{D(\sqrt{\phi})}{\sqrt{\phi}} \ . \tag{A9}$$

[Note that there is no factor of 2 in Eq. (A9) because the density of states (A8) is for $-1\leq\epsilon\leq 1$, while in Eq. (A9) $0\leq\phi\leq 1$.]

APPENDIX B: EVALUATION OF THE EXCHANGE INTEGRAL FOR ANISOTROPIC WAVE FUNCTIONS IN HEITLER-LONDON APPROXIMATION

In order to see qualitatively the effects of anisotropy of the envelope function it is instructive to carry through the calculation in the Heitler-London ap-

proximation. Even in this case, the evaluation of the integral is only approximate. Results for the distribution of exchange couplings are obtained using two complementary methods to evaluate the integrals. These are found to be within a few percent of each other over the values of exchange of interest.

In the Heitler-London approximation, using the Kohn-Luttinger (unperturbed) $1s$ wave functions

$$F_z(\vec{r}\,) = \frac{1}{(\pi a^2 b)^{1/2}} \exp[-(x^2/a^2 + y^2/a^2 + z^2/b^2)^{1/2}] \tag{B1}$$

(and similarly F_x and F_y), we obtain

$$j_{zz}(\vec{R}) = \int d^3r_1' d^3r_2' F_z(\vec{r}_1\,') F_z(\vec{r}_2\,' - \vec{R}) \frac{e^2}{\epsilon |\vec{r}_1\,' - \vec{r}_2\,'|} F_z(\vec{r}_2\,') F_z(\vec{r}_1\,' - \vec{R}) \ . \tag{B2}$$

Scaling the lengths in the three directions by the respective Kohn-Luttinger radii, thus $x_i = x_i'/a$, $y_i = y_i'/b$, and $z_i = z_i'/b\,(i = 1, 2)$, we get

$$j_{zz}(\vec{R}) = \frac{e^2}{\epsilon \pi^2 a} \int d^3r_1 d^3r_2 \frac{\exp[-(r_1 - |\vec{r}_1 - \vec{r}|)]\exp[-(r_2 - |\vec{r}_2 - \vec{r}|)]}{[|\vec{r}_1 - \vec{r}_2|^2 - (1 - b^2/a^2)(z_1 - z_2)^2]^{1/2}} \ , \tag{B3}$$

where $\vec{r} = (X/a, Y/a, Z/b)$. The major dependence of j_{zz} on $\vec{R}$ comes from the exponential terms in the numerator of the integrand. Thus, in order to evaluate the integral in Eq. (B3) approximately we may use the angularly averaged value of the denominator, which is

$$\left\langle \left[\frac{1}{|\vec{r}_1 - \vec{r}_2|^2 - (1 - b^2/a^2)(z_1 - z_2)^2} \right]^{1/2} \right\rangle_{\text{ang}} = \frac{1}{|\vec{r}_1 - \vec{r}_2|} \frac{1}{(1 - b^2/a^2)^{1/2}} \sin^{-1}[(1 - b^2/a^2)^{1/2}] \ ,$$

giving

$$j_{zz}(\vec{R}) = \frac{e^2}{\epsilon a} \frac{1}{(1 - b^2/a^2)^{1/2}} \{\sin^{-1}[(1 - b^2/a^2)^{1/2}]\} j_H(r) \ , \tag{B4}$$

where

$$j_H(r) = \tfrac{1}{5}\{-e^{-2r}(-\tfrac{25}{8} + \tfrac{23}{4}r + 3r^2 + \tfrac{1}{3}r^3) + (6/r)[S^2(\gamma + \ln r) + S'^2 \mathrm{Ei}(-4r) - 2SS'\mathrm{Ei}(-2r)]\} \tag{B5}$$

is the hydrogenic result in atomic units.[24] In Eq. (B5) $\gamma = 0.5772, \ldots,$ is Euler's constant, Ei the exponential integral, and $S = e^{-r}(1 + r + \frac{1}{3}r^2), S' = e^r(1 - r + \frac{1}{3}r^2)$.

Alternatively, at large separations ($R >> a, b$), we may replace the denominator by the value appropriate for the line joining the two donors, around which the maximum contribution to the exchange arises:

$$\left[\frac{1}{|\vec{r}_1 - \vec{r}_2|^2 - (1 - b^2/a^2)(z_1 - z_2)^2} \right]^{1/2} \rightarrow \frac{1}{[1 - (1 - b^2/a^2)\cos^2\theta]^{1/2}} \frac{1}{|\vec{r}_1 - \vec{r}_2|} \ ,$$

where θ is the polar angle of $\vec{r}$, related to the polar angle θ' of $\vec{R}$ by

$$\cos\theta = \left[1 + \frac{b^2}{a^2}\tan^2\theta'\right]^{-1/2} \ ,$$

so

$$j_{zz}(\vec{R}) = \frac{e^2}{\epsilon a}\left[\frac{a^2}{b^2}\cos^2\theta' + \sin^2\theta'\right]^{1/2} j_H(r) \ . \tag{B6}$$

Similar expressions are obtained for j_{xx} and j_{yy} by appropriate permutations of x, y, and z. The total exchange, averaging over the rapidly oscillating phase factors, is given by Eq. (A7):

$$\langle J(\vec{R}) \rangle = \tfrac{1}{18}[j_{xx}(\vec{R}) + j_{yy}(\vec{R}) + j_{zz}(\vec{R})] \ . \tag{B7}$$

Results obtained for the distribution function using Eqs. (B4) and (B6) differ from each other by even less than the few percent error resulting from usage of the spherically symmetric exchange interaction, and thus either may be used.

APPENDIX C: PROBABILITY DISTRIBUTION OF EXCHANGE COUPLINGS

To obtain the probability distribution of the strongest neighbor with an exchange value of J we assume that it is located a distance R from the spin at the origin. The value of R is clearly bounded by $R_H(J)$ where

$$j_s(R_H)=J \quad . \tag{C1}$$

The probability of finding a neighbor with an exchange between J and $J+dJ$ is weighted by the probability of finding the appropriate value of ϕ. This is given by $N(\phi_J)(d\phi_J/dJ)dJ$ with $\phi_J=J/j_s(R)$ and the distribution function N is calculated in Appendix A. If this neighbor is to be the strongest magnetic neighbor then we must multiply by the probability that there is no neighbor with an exchange value greater than J. This probability is $\exp(-n_D\Omega_J)$ where Ω_J is volume out to a distance $R_H(J)$ weighted by the fraction of exchange values greater than J in this volume. Thus

$$\Omega_J=4\pi\int_0^{R_H(J)} R'^2dR'\int_{J/j_s(R')}^{1} N(\phi)d\phi \quad . \tag{C2}$$

Finally we obtain the result

$$p(J)=4\pi n_D\int_0^{R_H(J)} R^2dRN(\phi_J)j_s^{-1}(R) \times \exp(-n_D\Omega_J) \tag{C3}$$

quoted in Eq. (4.14).

The nearest-neighbor distribution can be obtained by a similar argument with the modification that the volume Ω_J is replaced by the volume of the sphere of radius R weighted, of course, by a factor of unity. The result is quoted in Eq. (4.16).

---

*Present address: Technical University, Munich, West Germany.

†Present address: California Institute of Technology, Physics Department, Pasadena, Calif. 91125.

[1]For a general discussion of these phenomena see N. Mott, *Metal-Insulator Transitions* (Taylor and Francis, London, 1974); *Proceedings of the International Conference on Impurity Bands in Semiconductors* [Philos. Mag. B 42, No. 6 (1980)].

[2]C. Yamanouchi, K. Mizoguchi, and W. Sasaki, J. Phys. Soc. Jpn. 22, 859 (1967). Note, however, that we use a different concentration scale based on the Irvin curve [J. C. Irvin, Bell System Technical Journal 41, 387 (1962)]. For details see Ref. 3.

[3]G. A. Thomas, M. Capizzi, F. DeRosa, R. N. Bhatt, and T. M. Rice, Phys. Rev. B 23, 5472 (1981); M. Capizzi, G. A. Thomas, F. DeRosa, R. N. Bhatt, and T. M. Rice, Solid State Commun. 31, 611 (1979).

[4]W. Kolos and L. Wolniewicz, J. Chem. Phys. 43, 2429 (1965); J. Mol. Spectrosc. 54, 303 (1975).

[5]C. Herring and M. Flicker, Phys. Rev. 134, A362 (1964).

[6]V. Cannella and J. A. Mydosh, Phys. Rev. B 6, 4220 (1972).

[7]J. R. Marko and J. D. Quirt, Phys. Status Solidi B 64, 325 (1974).

[8]W. Sasaki, J. Phys. (Paris) 37, C4-307 (1976); W. Sasaki and J. Kinoshita, J. Phys. Soc. Jpn. 25, 1622 (1968).

[9]R. B. Kummer, R. E. Walstedt, S. Geschwind, V. Narayanamurti, and G. E. Devlin, Phys. Rev. Lett. 40, 1098 (1978); R. E. Walstedt, R. B. Kummer, S. Geschwind, V. Narayanamurti, and G. E. Devlin, J. Appl. Phys. 50, 1700 (1979).

[10]We define percolation here to be that temperature where exchange bonds $J > kT$ form an infinite cluster.

[11]R. N. Bhatt and T. M. Rice, Philos. Mag. B 42, 859 (1980).

[12]All samples except sample B were from the same source material as was employed in the work of Ref. 3, where further characterization of this material may be found.

[13]K. Andres, Cryogenics 18, 473 (1978).

[14]T. F. Rosenbaum, K. Andres, and G. A. Thomas, Solid State Commun. 33, 663 (1980).

[15]W. Kohn, in *Solid State Physics,* edited by F. Seitz and D. Turnbull (Academic, New York, 1957), Vol. 5, p. 257; R. A. Faulkner, Phys. Rev. 184, 713 (1969).

[16]M. Rosso, Phys. Rev. Lett. 44, 1541 (1980).

[17]We remark here that the topology of the clusters as defined here with respect to the central spin is very different from that of the clusters defined in Ref. 9 and in the next section. Thus a detailed comparison of the two methods of calculation is not feasible.

[18]R. Fisch, Phys. Rev. B 22, 3459 (1980).

[19]T. F. Rosenbaum, K. Andres, G. A. Thomas, and R. N. Bhatt, Phys. Rev. Lett. 45, 1723 (1980).

[20]R. A. Klemm, J. Phys. C 12, L735 (1979).

[21]A. J. Bray and M. A. Moore, J. Phys. C 13, L655 (1980).

[22]G. S. Grest and E. F. Gabl, Phys. Rev. Lett. 43, 1182 (1979); S. Nagata, R. R. Galazka, D. P. Mullin, H. Akbarzadeh, G. D. Khattak, J. K. Furdyna, and P. H. Keesom, Phys. Rev. B 22, 3331 (1980); R. R. Galazka, S. Nagata, and P. H. Keesom, *ibid.* 22, 3344 (1980).

[23]This is also indicated in recent renormalization-group calculations of R. N. Bhatt and P. A. Lee, in Proceedings of the Magnetism and Magnetic Materials Conference, Dallas, 1980 [J. Appl. Phys., 1981 (in press)].

[24]J. C. Slater, *Quantum Theory of Molecules and Solids* (McGraw-Hill, New York, 1963), Vol. I, p. 50.